A fast method for computing convolutions with structural Green's functions: application to tyre dynamic contact problems

Rabie Meftah, Denis Duhamel, Julien Cesbron, Yin Hai-Ping

A fast method for computing convolutions with structural Green's functions : application to tire dynamic contact problems

Rabie Meftah[a,*], Denis Duhamel[a], Julien Cesbron[b], Honoré Yin[a]

[a] *Université Paris-Est, laboratoire Navier,*
ENPC,IFSTTAR, CNRS, UMR 8205,
6 et 8 Avenue Blaise Pascal,
Cité Descartes, Champs sur Marne,
77455 Marne la Vallée, cedex 2, France
email : rabie.meftah@gmail.com,{denis.duhamel,hp.yin}@enpc.fr
[b] *LUNAM UNIVERSITÉ, IFSTTAR, IM, EASE, F. 44344, Bouguenais , France.*
email : julien.cesbron@ifsttar.fr

Abstract

Tire/road contact is the main source of car noise at speeds greater than 50 km/h. In this context, we have developed a new approach for modeling tire vibrations and the contact with rigid road surfaces during rolling. For tires, a periodic model is used to compute Green's functions. The response of tires can thus be modeled over a large frequency range. Then a fast convolution and a new contact model are developed and examples of computations of contact forces are given for real road textures. Spectra of forces for different tire velocities are also computed.

Keywords:
dynamic contact /tire/road/ Green's function/ convolution/ identification

*Corresponding author, rabie.meftah@gmail.com.

1. Introduction

The prediction of tire road noise needs both a tire vibration model and a method for computing the contact forces between a tire and a road.

For the tire vibrations, the simplest approach is the circular ring model as in [1]. However, for complex geometrical or material properties of the tire, a finite element model is much more appropriate. To avoid the heavy three-dimensional computations of [2], several efficient models have been proposed such as the wave finite element approach in [3] or the recursive method presented in [4, 5].

Here the dynamic response of the tire is calculated by convolution of the contact forces with the Green's functions of the tire. The convolution technique for contact problems is used by many authors : M. McIntyre al. [6] have applied the approach to the string/bow contact to study large-amplitude oscillations of musical instruments. C. Wang and J. Kim. [7, 8] have used the same approach for a thin beam impacting against a stop, A. Nordborq [9] for the wheel/rail contact problem and many other authors have used this technique in the tyre/road contact [10, 11, 12].

For orthotropic plates such Green's functions were analytically found in [13], but here they are found from the recursive model [4]. However the computation of the convolution can be time consuming. In this work we have used a different method. First it consists in the modal expansion of the pre-calculated Green's functions. The modal parameters are then used to construct a new convolution which allows quicker calculations than the traditional convolution. Then modal convolution is adapted to dynamic contact problems by using a kinematic contact condition.

The outline of the paper is thus the following. In section 2, the contact model, including the fast convolution and the kinematic contact condition is described. Then in section 3, a simple one-dimensionnel model is used as example to illustrate the advantages of this contact model. Then a 3D finite element model of the tire is presented and its Green's functions are computed. Finally, section 4 gives numerical results of displacements and contact forces for two road textures.

2. Contact model

A linear discretized dynamic problem can be generally expressed by a second order differential equation in the time domain:

$$\mathbf{M}\ddot{\mathbf{u}}(t) + \mathbf{C}\dot{\mathbf{u}}(t) + \mathbf{K}\mathbf{u}(t) = \mathbf{q}(t) \tag{1}$$

where $\mathbf{M}$, $\mathbf{C}$, $\mathbf{K}$, $\mathbf{u}$ and $\mathbf{q}$ are the mass matrix, the damping matrix, the stiffness matrix, displacement and force, respectively. In the frequency domain, the problem can be written:

$$\hat{\mathbf{u}}(\omega) = \hat{\mathbf{g}}(\omega)\ \hat{\mathbf{q}}(\omega) \tag{2}$$

where $\hat{\mathbf{g}}$ is the Green function :

$$\hat{\mathbf{g}}(\omega) = \left[-\omega^2\mathbf{M} + j\omega\mathbf{C} + \mathbf{K}\right]^{-1} \tag{3}$$

The traditional method when the time Green's function $\mathbf{g}(t)$ is known, is to calculate the dynamic response of the system by convolving the force with the Green's function:

$$\mathbf{u}(t) = \int_0^t \mathbf{g}(t-\tau)\mathbf{q}(\tau)\mathrm{d}\tau \tag{4}$$

For a unilateral contact between a dynamic system (tire) and a rigid body (road), both force $q(t)$ and displacement $u(t)$ are unknown. In addition to the convolution equation (4), the following contact conditions must be verified:

$$u(t) = u^r(t)\ ;\ q(t) > 0 \tag{5}$$

$$u(t) > u^r(t)\ ;\ q(t) = 0 \tag{6}$$

where u^r is the vertical road position (only vertical displacements are considered here).

2.1. Fast convolution

The computation of the response of the tire by a standard convolution requires a large number of coefficients. Here we try to reduce the computing time by simplifying the Green's function which can be approximated by a linear combination of N_m modes (not necessarily the true modes) as:

$$\hat{g}_{ij}(\omega) = \sum_{k=1}^{k=N_m} \frac{A_{ij}^k}{-\omega^2 + 2\sqrt{-1}\,\xi_{ij}^k \omega_{ij}^k \omega + {\omega_{ij}^k}^2} \tag{7}$$

Knowing $\hat{g}_{ij}(\omega)$ by a finite element model or by measurements, we must identify the residues A_{ij}^k, the dampings ξ_{ij}^k and the resonance frequencies ω_{ij}^k.There are several methods to solve this problem. In this study the LSCE (Least Squares Complex Exponential) is used. The principle of this algorithm is detailed in Appendix A.

By taking the analytical inverse Fourier transform, the Green's function in the time domain can be found by:

$$g_{ij}(t) = \sum_{k=1}^{k=N} \frac{A_{ij}^k}{\omega_{ij}^{dk}} e^{-\xi_{ij}^k \omega_{ij}^k} H(t) \tag{8}$$

with:

$$\omega_{ij}^{dk} = \omega_{ij}^k \sqrt{1 - {\xi_{ij}^k}^2}$$

and $H(t)$ is the Heaviside step function:

$$\begin{aligned} H(t) &= 0 \quad \text{for} \quad t < 0 \\ H(t) &= 1 \quad \text{for} \quad t \geq 0 \end{aligned} \tag{9}$$

The displacement $\mathbf{u}(t)$ is obtained from the contact force $\mathbf{q}(t)$ by the convolution:

$$\mathbf{u}(t) = \int_0^t \mathbf{g}(\tau)\mathbf{q}(t-\tau)d\tau = \int_0^t \mathbf{g}(t-\tau)\mathbf{q}(\tau)d\tau \tag{10}$$

Inserting expression (8) for $g_{ij}(t)$ in Eq. (10) yields to the displacement at point i :

$$u_i(t) = \sum_{j=1}^{j=N_p} \int_0^t \sum_{k=1}^{k=N} \frac{A_{ij}^k}{\omega_{ij}^{dk}} e^{-\xi_{ij}^k \omega_{ij}^k (t-\tau)} \left[sin\left(\omega_{ij}^{dk}\,(t-\tau)\right)\right] q_j(\tau)d\tau \tag{11}$$

where N_p is the size of displacements $\mathbf{u}$.

Separating the t and τ variables and rearranging, the displacement can be written as:

$$u_i(t) = \sum_{j=1}^{j=N_p} \sum_{k=1}^{k=N} \frac{A_{ij}^k}{\omega_{ij}^{dk}} e^{-\xi_{ij}^k \omega_{ij}^k t} \left[sin\left(\omega_{ij}^{dk}\, t\right)\alpha_{ij}^k(t) - cos\left(\omega_{ij}^{dk}\, t\right)\beta_{ij}^k(t)\right] \tag{12}$$

where $\alpha_{ij}^k(t)$ and $\beta_{ij}^k(t)$ are computed by:

$$\alpha_{ij}^k(t) = \int_0^t e^{\xi_{ij}^k \omega_{ij}^k \tau} cos(\omega_{ij}^{dk}\,\tau) q_j(\tau)d\tau \tag{13}$$

$$\beta_{ij}^k(t) = \int_0^t e^{\xi_{ij}^k \omega_{ij}^k \tau} sin(\omega_{ij}^{dk}\,\tau) q_j(\tau)d\tau \tag{14}$$

The parameters $\alpha_{ij}^k(t + \Delta t)$ and $\beta_{ij}^k(t + \Delta t)$ can be computed by the discrete versions of Eq. (14) as:

$$\begin{aligned} \alpha_{ij}^k((n+1)\Delta t) &= \alpha_{ij}^k(n\Delta t) + e^{\xi_{ij}^k \omega_{ij}^k n\Delta t} cos(\omega_{ij}^{kd}\, n\Delta t) q_j(n\Delta t)\Delta t \\ \beta_{ij}^k((n+1)\Delta t) &= \beta_{ij}^k(n\Delta t) + e^{\xi_{ij}^k \omega_{ij}^k n\Delta t} sin(\omega_{ij}^{kd}\, n\Delta t) q_j(n\Delta t)\Delta t \end{aligned} \tag{15}$$

2.2. Kinematic contact conditions

When there is no contact, the contact force equals zero and the displacement can be computed by the fast convolution. When there is contact, conditions must be written to find the contact force. We propose here to write two conditions, one for the displacement and the other for the velocity.

Eq. (10) can be separated into a term depending on the past history of forces $u_h(t)$ and another term depending only on the present time step:

$$\mathbf{u}(t) = \underbrace{\int_0^{t-\Delta t} \mathbf{g}(t-\tau)\mathbf{q}(\tau)d\tau}_{\mathbf{u}_h(t)} + \int_0^{\Delta t} \mathbf{g}(\tau)\mathbf{q}(t-\tau)d\tau \tag{16}$$

The displacement in point i is :

$$u_i(t) = \sum_{j=1}^{j=N_p} \left[\underbrace{\int_0^{t-\Delta t} g_{ij}(t-\tau)q_j(\tau)d\tau}_{u_{ij}^h(t)} + \int_0^{\Delta t} g_{ij}(\tau)q_j(t-\tau)d\tau \right] \tag{17}$$

In the same way taking the derivative of Eq. (17) leads to an equation in term of the velocity $v(t)$:

$$v_i(t) = \sum_{j=1}^{j=N_p} \left[\underbrace{\int_0^{t-\Delta t} g'_{ij}(t-\tau)q_j(\tau)d\tau}_{v_{ij}^h(t)} + \int_0^{\Delta t} g'_{ij}(\tau)q_j(t-\tau)d\tau \right] \tag{18}$$

Denoting :

$$\mathbf{Y}(t) = \begin{bmatrix} u_1(t) \\ v_1(t) \\ \vdots \\ u_{N_p}(t) \\ v_{N_p}(t) \end{bmatrix} \quad ; \quad \mathbf{Y}_j^h = \begin{bmatrix} u_{1j}^h(t) \\ v_{1j}^h(t) \\ \vdots \\ u_{N_p j}^h(t) \\ v_{N_p j}^h(t) \end{bmatrix} \tag{19}$$

leads to:

$$\mathbf{Y}(t) = \sum_{j=1}^{j=N_p} \mathbf{Y}_j^h(t) + \Psi(\mathbf{q}(t)) \tag{20}$$

where Ψ is an integral operator giving the influence of the contact force at the present time on the displacement and the velocity. So the contact conditions are:

$$\mathbf{Y} = \mathbf{Y}^r = [u_1^r(t) \quad \frac{du_1^r(t)}{dt} \quad ... \quad u_{N_p}^r(t) \quad \frac{du_{N_p}^r(t)}{dt}]^T \tag{21}$$

where $u_i^r(t)$ and $\frac{du_i^r(t)}{dt}$ are the position of the road and its velocity at point i as seen in the tire reference system. Using the modal decomposition for the displacement, Eq. (12) yields to the following expression :

$$\begin{aligned} v_i(t) = \quad & - \sum_{j=1}^{j=N_p} \sum_{k=1}^{k=N} \frac{A_{ij}^k \xi_{ij}^k \omega_{ij}^k}{\omega_{ij}^{dk}} e^{-\xi_{ij}^k \omega_{ij}^k t} \left[sin\left(\omega_{ij}^{dk}\, t\right) \alpha_{ij}^k(t) - cos\left(\omega_{ij}^{dk}\, t\right) \beta_{ij}^k(t) \right] \\ & + \sum_{j=1}^{j=N_p} \sum_{k=1}^{k=N} A_{ij}^k e^{-\xi_{ij}^k \omega_{ij}^k t} \left[cos\left(\omega_{ij}^{dk}\, t\right) \alpha_{ij}^k(t) + sin\left(\omega_{ij}^{dk}\, t\right) \beta_{ij}^k(t) \right] \end{aligned} \tag{22}$$

$\mathbf{u}^h(t)$ and $\mathbf{v}^h(t)$ are obtained from Eq. (12) and (22) by computing α and β with $\mathbf{q} = \mathbf{0}$ at the present time. The real value of this force $\mathbf{q}(t)$ at present time is such that:

$$\begin{aligned}
\Delta\mathbf{Y} &= \mathbf{Y}_r - \mathbf{Y}^h \\
&= \sum_{j=1}^{j=N_p} \begin{bmatrix}
\int_{t-\Delta t}^{t} \sum_{k=1}^{k=N} \frac{A_{1j}^k}{\omega_{1j}^{dk}} e^{-\xi_{1j}^k \omega_{1j}^k (t-\tau)} \left[sin\left(\omega_{1j}^{dk}\,(t-\tau)\right)\right] q_j(\tau) d\tau \\
\int_{t-\Delta t}^{t} \sum_{k=1}^{k=N} \frac{A_{1j}^k}{\omega_{1j}^{dk}} e^{-\xi_{1j}^k \omega_{1j}^k (t-\tau)} \left[-\xi_{1j}^k \omega_{1j}^k sin\left(\omega_{1j}^{dk}\,(t-\tau)\right) + \omega_{1j}^{dk} cos\left(\omega_{1j}^{dk}\,(t-\tau)\right)\right] q_j(\tau) d\tau \\
\vdots \\
\int_{t-\Delta t}^{t} \sum_{k=1}^{k=N} \frac{A_{N_p j}^k}{\omega_{N_p j}^{dk}} e^{-\xi_{N_p j}^k \omega_{N_p j}^k (t-\tau)} \left[sin\left(\omega_{N_p j}^{dk}\,(t-\tau)\right)\right] q_j(\tau) d\tau \\
\int_{t-\Delta t}^{t} \sum_{k=1}^{k=N} \frac{A_{N_p j}^k}{\omega_{N_p j}^{dk}} e^{-\xi_{N_p j}^k \omega_{N_p j}^k (t-\tau)} \left[-\xi_{N_p j}^k \omega_{N_p j}^k sin\left(\omega_{N_p j}^{dk}\,(t-\tau)\right) + \omega_{N_p j}^{dk} cos\left(\omega_{N_p j}^{dk}\,(t-\tau)\right)\right] q_j(\tau) d\tau
\end{bmatrix}
\end{aligned}$$

The integrals can be computed by Gauss quadratures with two points. The values of the forces at these two Gauss points are obtained by:

$$\mathbf{q} = \begin{bmatrix} q_1^1 \\ q_1^2 \\ \vdots \\ q_{N_p}^1 \\ q_{N_p}^2 \end{bmatrix} = \left(\sum_{k=1}^{k=N} \begin{bmatrix} \Psi_{11}^k & \cdots & \Psi_{1N_p}^k \\ \vdots & \vdots & \vdots \\ \vdots & \vdots & \vdots \\ \Psi_{N_p 1}^k & \cdots & \Psi_{N_p N_p}^k \end{bmatrix} \right)^{-1} \begin{bmatrix} du_1 \\ dv_1 \\ \vdots \\ du_{N_p} \\ dv_{N_p} \end{bmatrix} \tag{23}$$

with Ψ a 2*x*2 matrix defined by:

$$\Psi_{ij}^{k11} = \frac{A_{ij}^k}{\omega_{ij}^{kd}} e^{\xi_{ij}^k \omega_{ij}^k (t-t_1)} sin(\omega_{ij}^{kd}(t-t_1))\ \frac{\Delta t}{2} \tag{24}$$

$$\Psi_{ij}^{k12} = \frac{A_{ij}^k}{\omega_{ij}^{kd}} e^{\xi_{ij}^k \omega_{ij}^k (t-t_2)} sin(\omega_{ij}^{kd}(t-t_2))\ \frac{\Delta t}{2} \tag{25}$$

$$\Psi_{ij}^{k21} = \frac{A_{ij}^k}{\omega_{ij}^{dk}} e^{-\xi_{ij}^k \omega_{ij}^k (t-t_1)} \left[-\xi_{ij}^k \omega_{ij}^k sin\left(\omega_{ij}^{dk}\,(t-t_1)\right) + \omega_{ij}^{dk} cos\left(\omega_{ij}^{dk}\,(t-t_1)\right)\right]\ \frac{\Delta t}{2} \tag{26}$$

$$\Psi_{ij}^{k22} = \frac{A_{ij}^k}{\omega_{ij}^{dk}} e^{-\xi_{ij}^k \omega_{ij}^k (t-t_2)} \left[-\xi_{ij}^k \omega_{ij}^k sin\left(\omega_{ij}^{dk}\,(t-t_2)\right) + \omega_{ij}^{dk} cos\left(\omega_{ij}^{dk}\,(t-t_2)\right)\right]\ \frac{\Delta t}{2} \tag{27}$$

with

$$\begin{aligned}
t_1 &= t + \left(1 - \frac{1}{\sqrt{3}}\right)\frac{\Delta t}{2} \\
t_2 &= t + \left(1 + \frac{1}{\sqrt{3}}\right)\frac{\Delta t}{2}
\end{aligned} \tag{28}$$

From the knowledge of the contact forces at times t_1 and t_2, the parameters $\alpha_{ij}^k(t+\Delta t)$ and $\beta_{ij}^k(t+\Delta t)$ can be computed by Eq. (15). The number of contact points can change with time. The contact occurs when $u^h(t) \leq u^r(t)$ for each point in the contact zone. Eq. (21) for the points where the contact happens allows to determine the contact forces at these points.

3. A simple one-dimensional model

3.1. Description of the model

To illustrate the approach presented above, let us consider a simple dynamic contact problem. The purpose of this example is to test the fast convolution method, to compare it with the traditional convolution and to test the kinematic contact conditions. The simplest dynamic system considered in vibration problems is the Single Degree of Freedom (SDoF) oscillator. In this example, the system moves through a profile $u^r(x)$ with a constant speed $V_0 = 0.1$ m.s^{-1}. It is supposed that the displacement occurs without slipping as shown in figure (A.1).

[Figure 1 about here.]

Consider a sinusoidal profile for the road :

$$u_r = A_0 \sin(kx) = A_0 \sin(\frac{2\pi}{\lambda_r} V_0 t) \tag{29}$$

where $\lambda_r = 10$ *mm* is the wavelength of the profile and $A_0 = 5$ *mm* its amplitude.

The system verifies the equations:

$$M\ddot{u} + C\dot{u} + Ku = -Mg + F_c \tag{30}$$
$$u(t) \geq u^r(t) \tag{31}$$
$$F_c \geq 0 \tag{32}$$

with the initial conditions:

$$u_0 = u(0) = u^r(0) \tag{33}$$
$$v_0 = \left.\frac{du(t)}{dt}\right|_{t=0} = 0 \tag{34}$$

The displacement $u(t)$ at time t depends on the contact forces history $F_c(t)$ imposed by the texture of the surface. Two situations arise: there is a contact between the system and the surface and the displacement of the system equals the height of the surface $u^r(t)$ and the velocities are also equal, or there is no contact and in this case the contact force is null and the displacement of the system is strictly higher than that of the surface.

If there is no contact, the displacement and contact forces are given by :

$$u(t) = e^{-\xi\omega_0(t-t_c)}\left[u_c \cos(\omega_d(t-t_c)) + \frac{v_c + \xi\omega_0 u_c}{\omega_d}\sin(\omega_d(t-t_c))\right] \tag{35}$$
$$F_c(t) = 0 \tag{36}$$

where u_c and v_c are respectively the displacement and velocity at the last contact instant t_c.

The result will also be compared with the case where a contact stiffness is included. In this case, if there is contact, the contact force is computed by (37) :

$$F_c(t) = k_c \Delta x = k_c\left[u^r(t) - u^h(t)\right] \tag{37}$$

where k_c is the contact stiffness.

3.2. Comparison with standard convolutions

The traditional method when the time Green's function $g(t)$ is known, is to calculate the dynamic response of the system by convolving the contact forces with the Green's function:

$$u(t) = \int_0^t g(t-\tau)q(\tau)\mathrm{d}\tau \tag{38}$$

Equation (38) can be discretized as follows:

$$u_k = \sum_{m=0}^{k} g_{k-m} q_m \tag{39}$$

Where u_k is the displacement at time $k\Delta t$.

Let's note N_t the number of time steps used to calculate the displacement, and N_g the number of time steps for the influencing Green's function. The effect of the Green's function is neglected when the amplitudes of oscillation at time greater than $N_g \Delta t$ are hundred times smaller than the maximum of the Green's function $g(t)$ (in this example the maximum amplitude is $2.5\ 10^{-4}\ mN^{-1}$).

Equation (39) is reduced to :

$$u_k = \sum_{m=0}^{\min(k,N_g)} g_{k-m} q_m \tag{40}$$

The parameters used in the model for the simulations are given in Table A.1.

[Table 1 about here.]

Using standard convolution is costly in terms of computing time, especially with a small time step. Indeed, from equations (40) and (12) we can see that in the case of a classical convolution, the number of calculation operations is proportional to the number of time steps N_t and to the size of the Green's functions N_g, while in the modal decomposition it is proportional to N_t and to the approximation order N_m. Table A.2 shows a comparison of computing times between both methods.

[Table 2 about here.]

3.3. Comparison with penalty methods

Figures (A.2), (A.3) and (A.4) show the displacements $u(t)$ and the contact forces $F_c(t)$ calculated by the penalty method and the present method for different values of the contact stiffness k_c. In the figures, we observe that the result obtained with the penalty method depends on the choice of the contact stiffness. If we use a low value of k_c, we obtain an unphysical solution (interpenetration phenomena) and if we use a high value, numerical instabilities appear. Finally, if we use a suitable value the results converge to those of the present method. In other words, the drawback of the penalty method is its instability due to the arbitrary choice of the contact stiffness, while the present method that only uses a kinematic condition is always stable.

[Figure 2 about here.]

[Figure 3 about here.]

[Figure 4 about here.]

4. Tire model

4.1. Tire section

The first step is to have a model for the vibrations of the tire. Here a periodic model has been developed. It consists in modeling a short cell of the tire as in Figure A.5 and using calculations on this cell for computing Green's functions as described below. Stiffness and mass matrices of a cell are obtained from commercial finite element software. In a first step they are obtained in a cartesian coordinate system and then they are transformed in a cylindrical coordinate system in which the whole structure is periodic.

The tire is also inflated with an internal pressure P. So its vibrations are considered as a small perturbation of the prestressed static state shown in Figure A.5. This prestress generates an additional stiffness matrix denoted K_P. So, the full dynamic stiffness matrix is given by:

$$\mathbf{D}^0(\omega) = \left[\mathbf{K}^0 + \mathbf{K}_P + j\omega\mathbf{C}^0 - \omega^2\mathbf{M}^0\right] \tag{41}$$

[Figure 5 about here.]

The tire studied here is of type Michelin 165/65/R13 77T. Its geometric properties are given in Table A.3. The mechanical properties of the different parts of the tire are given in Table A.4.

[Table 3 about here.]

[Table 4 about here.]

4.2. Reference cell

Consider a periodic structure consisting of N cells. Let's denote $\mathbf{t}$ the geometric transformation that connects the real cell and the reference cell (see Figure A.6). Denoting $\mathbf{x}_0^i$ the coordinates of node i of the real cell and $\mathbf{x}^i$ the coordinates of node i of the reference cell yields :

$$\begin{bmatrix} \mathbf{x}^1 \\ \vdots \\ \mathbf{x}^i \\ \vdots \\ \mathbf{x}^L \end{bmatrix} = \underbrace{\begin{bmatrix} \mathbf{t}^1 & 0 & 0 & 0 & 0 \\ \vdots & \ddots & & & \vdots \\ 0 & 0 & \mathbf{t}^i & 0 & 0 \\ \vdots & & & \ddots & \vdots \\ 0 & 0 & 0 & 0 & \mathbf{t}^L \end{bmatrix}}_{\mathbf{T}} \begin{bmatrix} \mathbf{x}_0^1 \\ \vdots \\ \mathbf{x}_0^i \\ \vdots \\ \mathbf{x}_0^L \end{bmatrix} \tag{42}$$

where $\mathbf{t}^i$ is the local transformation matrix of the node i and L is the number of nodes.

[Figure 6 about here.]

Therefore, the mass matrix $\mathbf{M}$ and the stiffness matrix $\mathbf{K}$ are calculated in the reference frame from the mass matrices ($\mathbf{M}^0$) and stiffness ($\mathbf{K}^0$) of the real cell by:

$$\mathbf{M} = \mathbf{T}\mathbf{M}^0\mathbf{T}^{-1} \tag{43}$$

$$\mathbf{K} = \mathbf{T}\left(\mathbf{K}^0 + \mathbf{K}_p\right)\mathbf{T}^{-1} \tag{44}$$

The dynamic stiffness matrix is calculated from the matrices and the damping matrix $\mathbf{C}$

$$\mathbf{D} = \mathbf{D}(\omega) = \mathbf{K} + j\omega\mathbf{C} - \omega^2\mathbf{M} \tag{45}$$

4.3. Equivalent matrix

The aim of the periodic model is to build the global dynamic stiffness matrix of the structure from the dynamic stiffness matrix of a single period. It is obtained by recursively eliminating the internal degrees of freedom between adjacent cells. Consider the dynamic stiffness matrices $\mathbf{D}^1$ and $\mathbf{D}^2$ of two neighbouring cells:

$$\mathbf{D}^1 = \begin{bmatrix} \mathbf{D}^1_{LL} & \mathbf{D}^1_{LR} \\ \mathbf{D}^1_{RL} & \mathbf{D}^1_{RR} \end{bmatrix} \; ; \; \mathbf{D}^2 = \begin{bmatrix} \mathbf{D}^2_{LL} & \mathbf{D}^2_{LR} \\ \mathbf{D}^2_{RL} & \mathbf{D}^2_{RR} \end{bmatrix} \tag{46}$$

The equivalent matrix of the two cells structure is obtained by eliminating the internal degrees of freedom by:

$$\mathbf{D}^{eq} = \begin{bmatrix} \mathbf{D}^1_{LL} - \mathbf{D}^1_{LR}\mathbf{D}^*\mathbf{D}^1_{RL} & -\mathbf{D}^1_{LR}\mathbf{D}^*\mathbf{D}^2_{LR} \\ -\mathbf{D}^2_{RL}\mathbf{D}^*\mathbf{D}^1_{RL} & \mathbf{D}^2_{RR} - \mathbf{D}^2_{RL}\mathbf{D}^*\mathbf{D}^2_{LR} \end{bmatrix} \tag{47}$$

with:

$$\mathbf{D}^* = \left[\mathbf{D}^1_{RR} + \mathbf{D}^2_{LL}\right]^{-1}$$

This operation is repeated n times with n such as :

$$N = \sum_{i=1}^{n} 2^{p_i} \; ; \; p_1 > p_2 > ... > p_n \tag{48}$$

with p_i the position of the i^{th} figure 1 in the binary representation of the number N of cells in the tire.

4.4. Green's functions

Consider the domain Ω of the tire. It can be separated into two subdomains Ω_l and Ω_c. The number of cells in the domain Ω_c where the contact occurs, is denoted by N_c. The other free part Ω_l of the tire has N_l cells, see Figures A.7 and A.8.

[Figure 7 about here.]

The dynamic stiffness matrix of domain Ω_l, denoted $\mathbf{D}^{eq}$, is computed by the method presented in section 4.3. Then the full dynamic stiffness matrix of the tire is computed by a standard finite element assembling between $\mathbf{D}^{eq}$ and the matrices of the N_c cells of Ω_c, see Figure A.8 and Eq. (49). The matrix of Green's functions is obtained by solving a linear system with Eq. (49) and different load cases associated to different points in the contact zone. The number of load cases is limited to the number of dofs in a section of the tire.

[Figure 8 about here.]

$$\underbrace{\begin{bmatrix} \mathbf{D}_{11} + \mathbf{D}^{eq}_{11} & \mathbf{D}_{12} & \mathbf{0} & \dots & \mathbf{D}^{eq}_{12} \\ \mathbf{D}_{21} & \mathbf{D}_{22} + \mathbf{D}_{11} & \ddots & \ddots & \ddots \\ \mathbf{0} & \ddots & \ddots & \ddots & \ddots \\ \vdots & \ddots & \ddots & \mathbf{D}_{11} + \mathbf{D}_{22} & \mathbf{D}_{12} \\ \mathbf{D}^{eq}_{21} & \ddots & \ddots & \mathbf{D}_{21} & \mathbf{D}_{22} + \mathbf{D}^{eq}_{22} \end{bmatrix}}_{\mathbf{D}_T} \tag{49}$$

Full tire is modeled using parameters summarized in Tables A.3 and A.4 with an internal pressure of 2 *bars*. Then Green's functions are calculated using the finite element software Abaqus. Figure A.9 shows an example of comparison of Green's function obtained by the periodic model and those obtained by Abaqus. The results show a good consistency between the two methods of calculation which confirms the correctness of the implementation of the dynamic stiffness matrix in the periodic method.

[Figure 9 about here.]

Each Green's function is approximated by a modal expansion. Modal parameters are identified by the LSCE algorithm presented in Appendix A. For each coefficient of the Green's matrix an optimal number of coefficient N_m is chosen to get the best approximation. To check the accuracy of estimated modal data, the Green's function is regenerated. This method aims to find the best estimates of modal data that minimizes the error defined in Eq. (50)

$$E = \frac{\int_0^{\omega_{max}} |G(\omega) - \sum_{k=1}^{k=N_m} \frac{A_k}{-\omega^2 + 2j\xi_k\omega\omega_k + \omega_k^2}| \mathrm{d}\omega}{\int_0^{\omega_{max}} |G(\omega)| \mathrm{d}\omega} \tag{50}$$

The error is low, generally below 5%. In Figure A.10, a Green's function and its approximation are presented for the coefficient with the maximal error (6.5%). One can see that the approximation is very good. In this example we consider ten sections, each section contains thousand 1034 nodes, and each Green function is approximated by around fifty modes ($N_m \sim 50$).

[Figure 10 about here.]

5. Road contact

5.1. Road textures

We assume that the roads are perfectly rigid and that the contact area remains constant with time. We consider two road textures which are measured in [14]. The measured area is $L = 2m$ long and $b = 0.35m$ width with a sampling of $dx = dy = 384\ \mu m$. Figure A.11 presents the samples of two different roads of sizes 0.1 m by 0.1 m, see [14] for other examples.

[Figure 11 about here.]

We want to compute the displacements and forces in the contact zones. The Green's functions of the tire are computed as in section 4.3 in the frequency range [0 4000 Hz]. The contact zone is changing as the tire is moving during the rolling process. The contact points are moving in the fixed coordinate system as:

$$\begin{aligned} x &= x_0 + V_0 t \\ y &= y_0 \\ z &= u^r(x, y) \end{aligned} \tag{51}$$

where (x_0, y_0, z_0) are the coordinates in the system moving at constant velocity V_0 with the tire. The maximal contact area is constant with time while the real contact area and the number of contact points can change.

5.2. Numerical results

All simulations are made for a contact length $L_c = 6\ cm$ and a width $l_c = 8\ cm$. The number of points is $N_x = 10$ along X and $N_y = 12$ along Y. The tire is rolling over a length $L = 2m$. The tread is discretized with steps $dX \approx dY \approx 5\ mm$ with an interpolation of the tire height between two tread points. Figures A.12 and A.13 present the displacements and stress for the two road surfaces of Figure A.11. The displacements have shapes similar to road textures. Losses of contact and high stress are seen at the maximal heights of asperities. Road (A) generates higher stress than road (B).

[Figure 12 about here.]

[Figure 13 about here.]

The stress level, denoted L_f and computed in decibels relatively to a reference value of $\sigma^0 = 10^2 N/m$, is obtained by:

$$L_f = 20 \log_{10} \left(\frac{|\sigma(\omega)|}{\sigma^0} \right) \tag{52}$$

Figures A.14 and A.15 present the third octave force spectra for roads (A) and (B) and for different velocities. When the velocity increases the spectra are shifted towards higher frequencies and the maximal level is also increased. The force level is quite significant for frequencies between 500 Hz and 5000 Hz. For road (A) the maximum level is obtained for 4000 Hz, while for road (B) it is for 2000 Hz. Globally the force level is higher for road (A) than for road (B). More examples can be found in [15].

[Figure 14 about here.]

[Figure 15 about here.]

6. Conclusion

A new approach of dynamic contact computation is developed to treat a tire road contact problem. For the tire, a periodic model is used to compute Green's function of the tire in the contact area. The model is validated by comparison to a classical finite element model. The periodic model leads to significant reduction of time computing. Then the contact model developed in this paper consist of the modal expansion of the modal expansion of the pre-calculated Green's functions. The modal parameters are then used to construct a new convolution which allows quicker calculations than the traditional convolution. The modal convolution is adapted to dynamic contact problems by using a kinematic contact condition. Contact model is validated in the case of an academic example by comparison to the penalty method. Both methods give the same result but the developed method is more stable and easier to implement. Results of the presented tire/road contact model show that the force levels are highly dependant on the texture levels and the rolling velocities. Increasing the rolling velocity clearly shifts the force levels towards higher frequencies and increases the global level. Force levels are also significant between 500 Hz and 5000 Hz.

References

[1] S.C. Huang and W. Soedel. Response of rotating rings to harmonic and periodic loading and comparison with the inverted problem. *Journal of Sound and Vibration*, 118(2):253–270, 1987.

[2] M. Brinkmeier, U. Nackenhorst, S. Petersen, and O. vonEstorff. A finite element approach for the simulation of tire rolling noise. *Journal of Sound and Vibration*, 309:20–39, 2008.

[3] Y. Waki, B.R. Mace, and M.J. Brennan. Free and forced vibrations of a tyre using a wave/finite element approach. *Journal of Sound and Vibration*, 323:737–756, 2009.

[4] D. Duhamel. A recursive approach for the finite element computation of waveguides. *Journal of Sound and Vibration*, 323(1-2):163–172, 2009.

[5] D. Duhamel, S. Erlicher, and H.H. Nguyen. A recursive finite element method for computing tyre vibrations. *European Journal of Computational Mechanics*, 20(1-4):9–27, 2011.

[6] M. McIntyre, R. Schumacher, and J. Woodhouse. On the oscillations of musical instruments. *Journal of the Acoustical Society of America*, 74:1325–1345, 1983.

[7] C. Wang and J. Kim. New analysis method for a thin beam impacting against a stop based on the full continuous mode. *Journal of Sound and Vibation*, 191(1-4):809–823, 1996.

[8] C. Wang and J. Kim. The dynamic analysis of a thin beam impacting against a stop of general three-dimensional geometry. *Journal of Sound and Vibation*, 203:237–249, 1997.

[9] A. Nordborg. Rail noise generation due to nonlinear effects and parametric excitation. *Journal of the Acoustical Society of America*, 111:1772–1781, 2002.

[10] K. Larsson. *Modelling of dynamic contact-exemplified on tire/road interaction*. PhD thesis, Chalmers University of Technology, Goteborg, Sweden,, 2002.

[11] F. Wullens. *Excitation of tyre vibration due to tyre/road interaction*. PhD thesis, Chalmers University of Technology, Goteborg, Sweden,, 2004.

[12] P.B.U. Andersson and W. Kropp. Time domain contact model for tyre/road interaction including nonlinear contact stiffness due to small-scale roughness. *Journal of Sound and Vibration*, pages 296–312, 2008.

[13] J. F. Hamet. Tire/road noise: time domain green's function for the orthotropic plate model. *Acta acoustica united with Acustica*, 87:470–474, 2001.

[14] Prediction and propagation of rolling noise. Technical report, Deufrako P2RN project, March 2009.

[15] R. Meftah. *Une approche par formalisme de Green réduit pour le calcul des structures en contact dynamique: application au contact pneumatique chaussée*. PhD thesis, Université Paris-Est, 2011.

Appendix A. LSCE algorithm

The Green's function $\hat{g}(\omega)$ is supposed to be known, $g(t)$ is its inverse Fourier transform. The Green's function in the frequency domain can be written in the form

$$\hat{g}(\omega) = \sum_{k=1}^{k=N} \left[\frac{R_k}{j\omega - \lambda_k} + \frac{R_k^*}{j\omega - \lambda_k^*} \right] \tag{A.1}$$

Denoting $R_{n+k} = R_k^*$ and $\lambda_{n+k} = \lambda_k^*$, the Green's function can be written as

$$\hat{g}(\omega) = \sum_{k=1}^{k=2N} \frac{R_k}{j\omega - \lambda_k} \tag{A.2}$$

Then by using an inverse Fourier transform, the Green's function in the time domain can be found as,

$$g(t) = \sum_{k=1}^{k=2N} R_k e^{\lambda_k t} \tag{A.3}$$

$g(t)$ is sampled by equally spaced time intervals Δt. At the time $n\Delta t$, the discrete Green's function can be written as

$$g(n\Delta t) = \sum_{k=1}^{k=2N} R_k e^{\lambda_k n\Delta t} \tag{A.4}$$

By setting $z_k = e^{\lambda_k \Delta t}$, the Green's function can be written as,

$$g(n\Delta t) = \sum_{k=1}^{k=2N} R_k z_k^n \tag{A.5}$$

We write $g(t)$ for different times $m\Delta t$ ($m = 1, 2...2N$)

$$\begin{aligned}
g_0 &= g(0) = \sum_{k=1}^{k=2N} R_k \\
g_1 &= g(\Delta t) = \sum_{k=1}^{k=2N} R_k z_k \\
g_2 &= g(2\Delta t) = \sum_{k=1}^{k=2N} R_k z_k^2 \\
&[...] \\
g_{2N} &= g(2N\Delta t) = \sum_{k=1}^{k=2N} R_k z_k^{2N}
\end{aligned} \tag{A.6}$$

We assume that z_k is the solution of the polynomial equation (A.7).

$$\beta_0 + \beta_1 z_k + \beta_2 z_k^2 + ...\beta_i z_k^i .... + \beta_{2N} z_k^{2N} = 0 \tag{A.7}$$

This equation is known as the Prony equation, and was developed by Gaspard Riche in 1975.
So, by multiplying equations (A.6) by corresponding β_i and taking a sum from $i = 1$ to $2N$

$$\sum_{i=0}^{i=2N} \beta_i g_i = \sum_{i=0}^{i=2N} (\beta_i \sum_{k=1}^{k=2N} R_k z_k^i) = \sum_{k=1}^{k=2N} (R_k \sum_{i=0}^{i=2N} \beta_i z_k^i) = 0 \tag{A.8}$$

Using equation (A.7), we can write

$$\beta_0 g(0) + \beta_1 g(\Delta t) + \beta_2 g(2\Delta t) + ...\beta_i g(i\Delta t).... + \beta_{2N} g(2N\Delta t) = 0 \tag{A.9}$$

If we know the Green's function at $4N$ time steps, we can build the Hankel matrix, then the $2N$ values of β_i can be found by resolving the matrix equation

$$\begin{bmatrix} g_0 & g_1 & g_2 & \cdots & g_{2N-1} \\ g_1 & g_2 & g_3 & \cdots & g_{2N} \\ \cdots & \cdots & \cdots & \cdots & \cdots \\ g_{2N-2} & g_{2N-1} & g_{2N} & \cdots & g_{4N-3} \\ g_{2N-1} & g_{2N} & g_{2N+1} & \cdots & g_{4N-2} \end{bmatrix} \begin{bmatrix} \beta_0 \\ \beta_1 \\ \cdots \\ \beta_{2N-2} \\ \beta_{2N-1} \end{bmatrix} = \begin{bmatrix} g_{2N} \\ g_{2N+1} \\ \cdots \\ g_{4N-2} \\ g_{4N-1} \end{bmatrix} \tag{A.10}$$

The number of rows in the equation (A.10) can be increased for a least square solution. By setting **H** the Hankel matrix, $\mathbf{b} = [\beta_0\, \beta_1 ....\beta_{2N}]^T$ and $\mathbf{h} = [g_{2N} ....g_{4N-1}]^T$, the $2N$ values of β_i are calculated as

$$\mathbf{b} = \left(\mathbf{H}^T\mathbf{H}\right)^{-1}\mathbf{H}^T\mathbf{h} \tag{A.11}$$

The z_k values can be found easily as roots of the polynomial equation (A.7). Then the natural frequencies ω_k and the damping ratios ξ_k are related to the z_k coefficients by

$$\omega_k = \frac{1}{\Delta t}\sqrt{\log(z_k)\log(z_k^*)} \tag{A.12}$$

$$\xi_k = \frac{-\log(z_k z_k^*)}{2\omega_r \Delta t} \tag{A.13}$$

To determine the residue values A_k, the Green's function can be expressed at different frequencies (Ω_1, Ω_2...),

$$\begin{bmatrix} \frac{1}{-\Omega_1^2+2j\xi_1\Omega_1\omega_1+\omega_1^2} & \cdots & \frac{1}{-\Omega_1^2+2j\xi_{2N}\Omega_1\omega_{2N}+\omega_{2N}^2} \\ \frac{1}{-\Omega_2^2+2j\xi_1\Omega_2\omega_1+\omega_1^2} & \cdots & \frac{1}{-\Omega_2^2+2j\xi_{2N}\Omega_2\omega_{2N}+\omega_{2N}^2} \\ \cdots & \cdots & \cdots \\ \frac{1}{-\Omega_{2N}^2+2j\xi_1\Omega_{2N}\omega_1+\omega_1^2} & \cdots & \frac{1}{-\Omega_{2N}^2+2j\xi_{2N}\Omega_{2N}\omega_{2N}+\omega_{2N}^2} \end{bmatrix} \begin{bmatrix} A_1 \\ A_2 \\ \cdots \\ A_{2N} \end{bmatrix} = \begin{bmatrix} \hat{g}(\Omega_1) \\ \hat{g}(\Omega_2) \\ \cdots \\ \hat{g}(\Omega_{2N}) \end{bmatrix} \tag{A.14}$$

The solution of this set of linear equations will yield the residues.

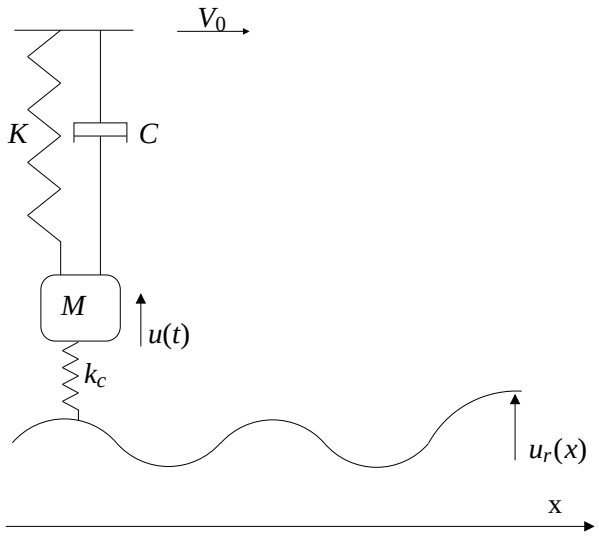

Figure A.1: SDOF mass-spring system on a sinusoidal surface

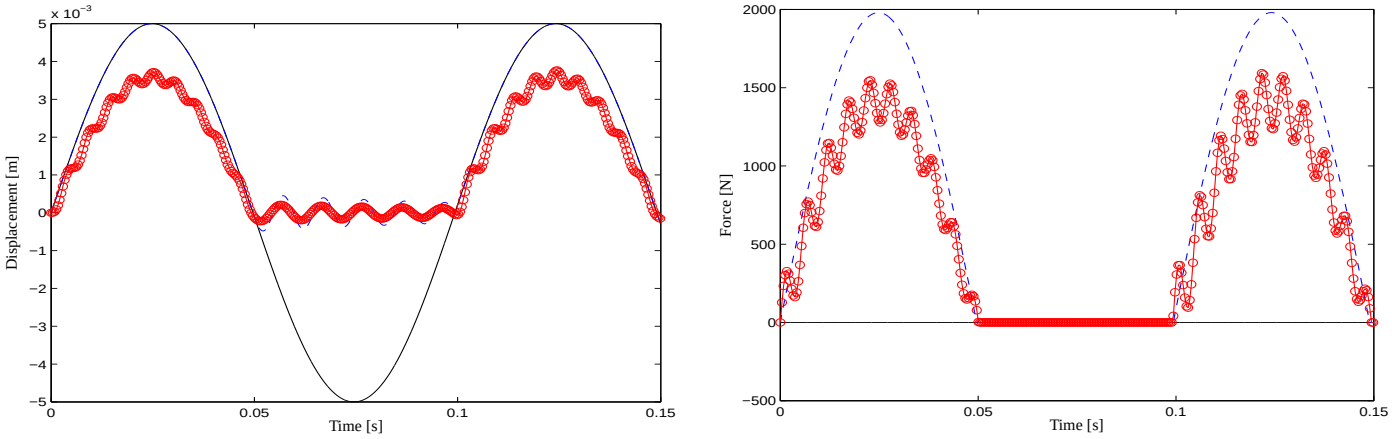

(a) (b)

Figure A.2: Displacement (a) and contact force (b) obtained by penalty (low contact stiffness $k_c = 10^6\ m/N$) and kinematic methods : —road profile, $-o-$ penalty method , $--$ kinematic method

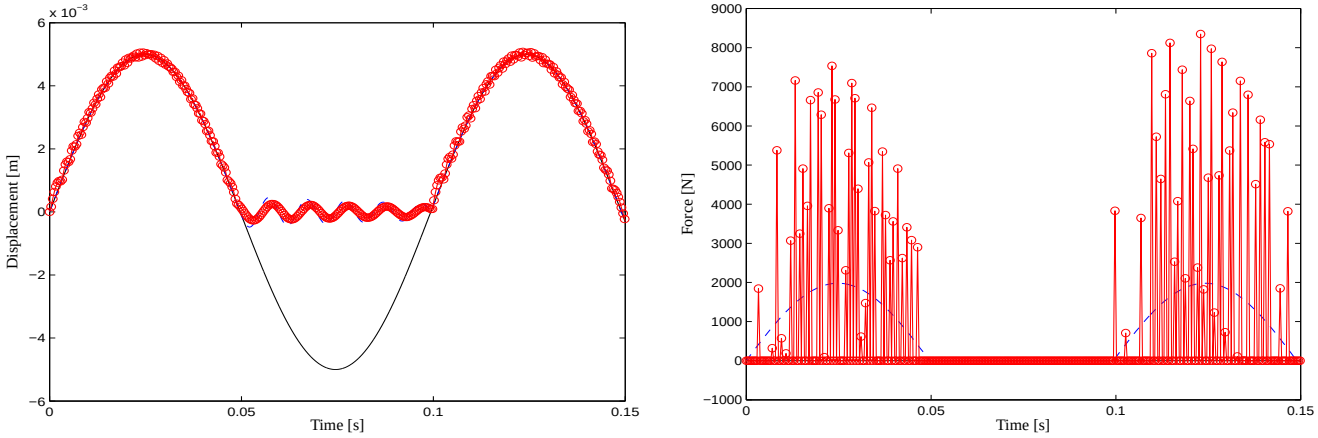

(a) (b)

Figure A.3: Displacement (a) and contact force (b) obtained by penalty (high contact stiffness $k_c = 10^8\ m/N$) and kinematic methods : —road profile, $-o-$ penalty method , $--$ kinematic method

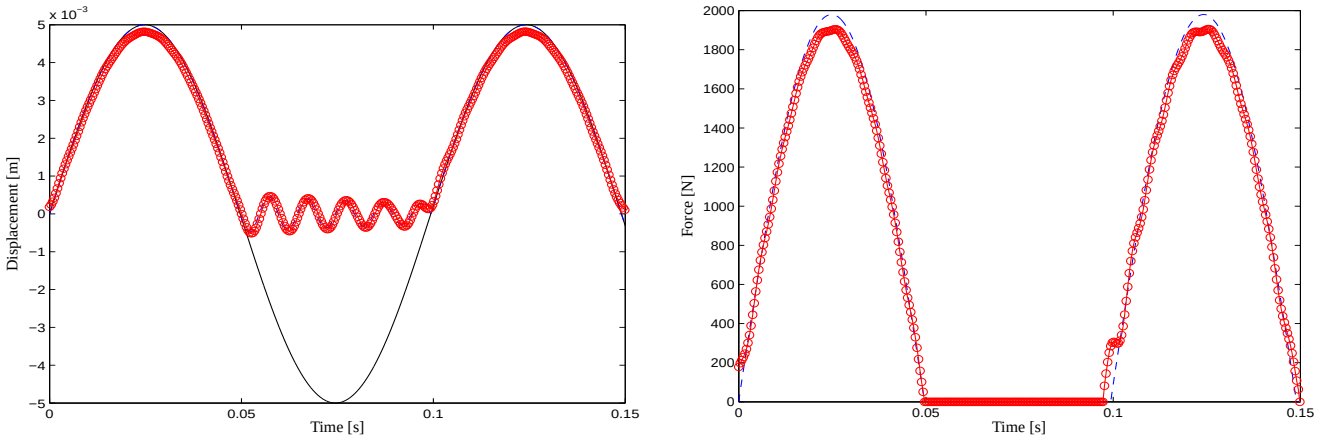

(a) (b)

Figure A.4: Displacement and contact force obtained by penalty (suitable contact stiffness $k_c = 10^7\ m/N$) and kinematic methods : —road profile, $-o-$ penalty method , $--$ kinematic method

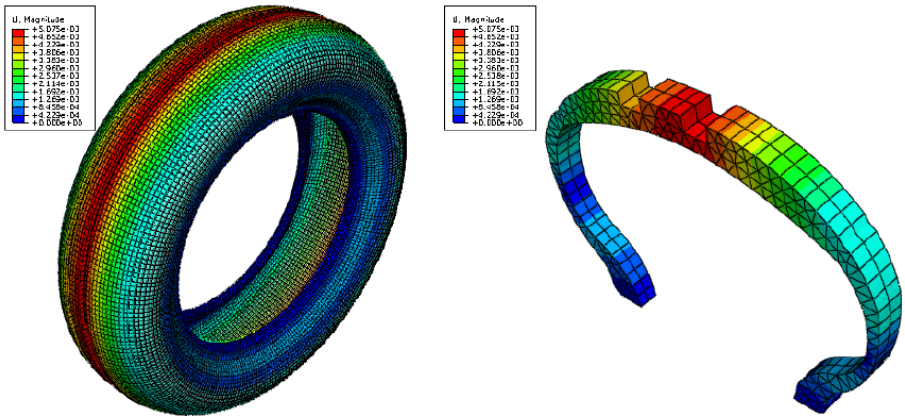

Figure A.5: Section of the tire and displacements for an inflation pressure of 2 *bars*.

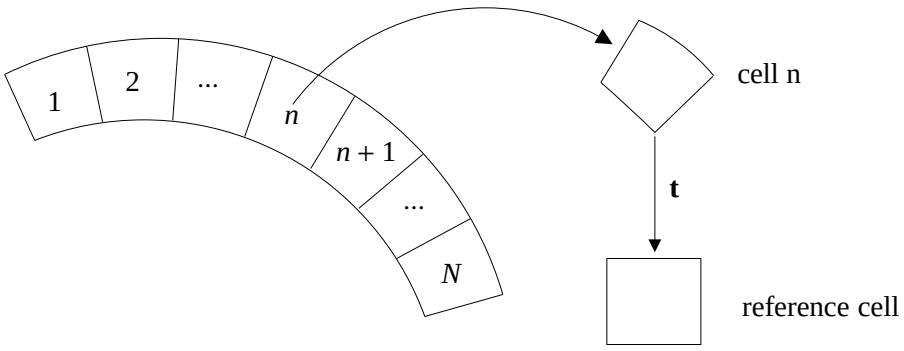

Figure A.6: Geometric transformation

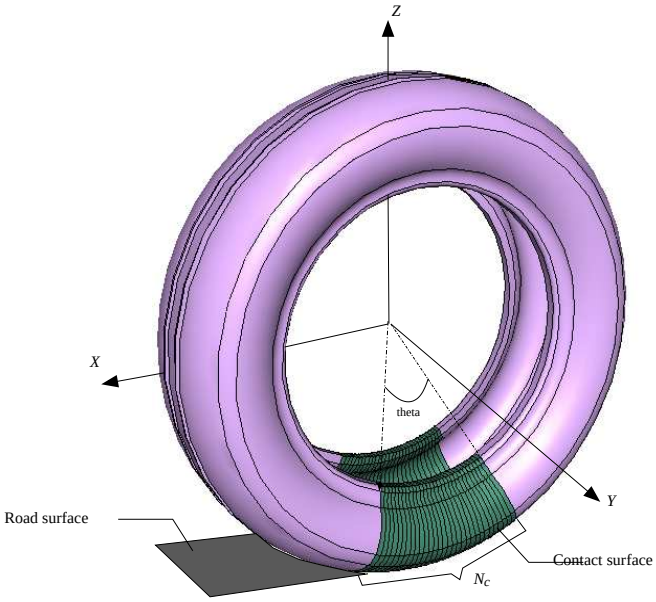

Figure A.7: Contact zone with the road.

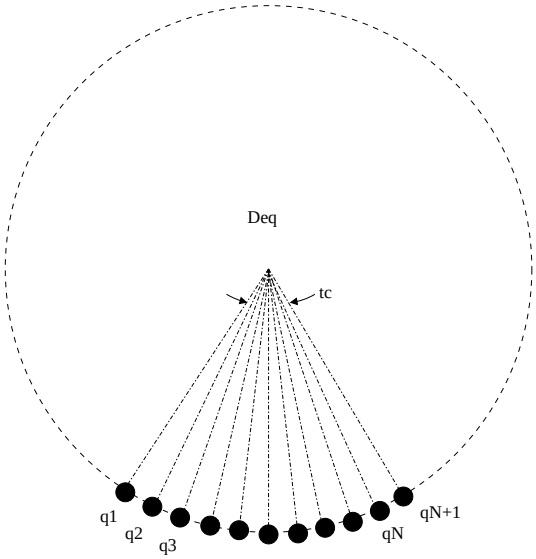

Figure A.8: Dofs of the global matrix.

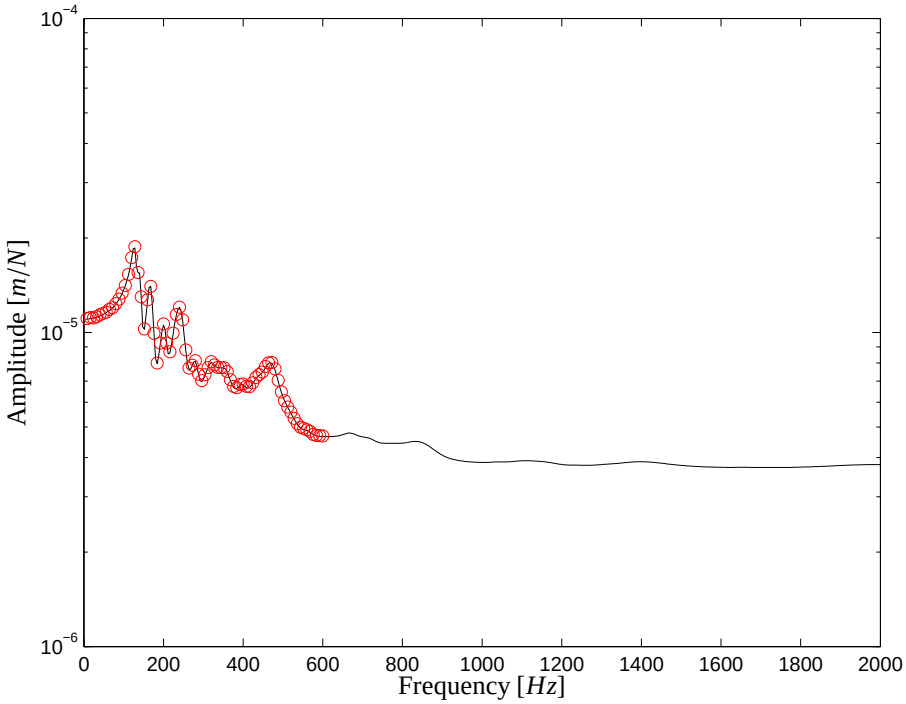

Figure A.9: Periodic model validation with internal pressure $P = 2\ bars$: – periodic model, $-o-$ full tire Abaqus model

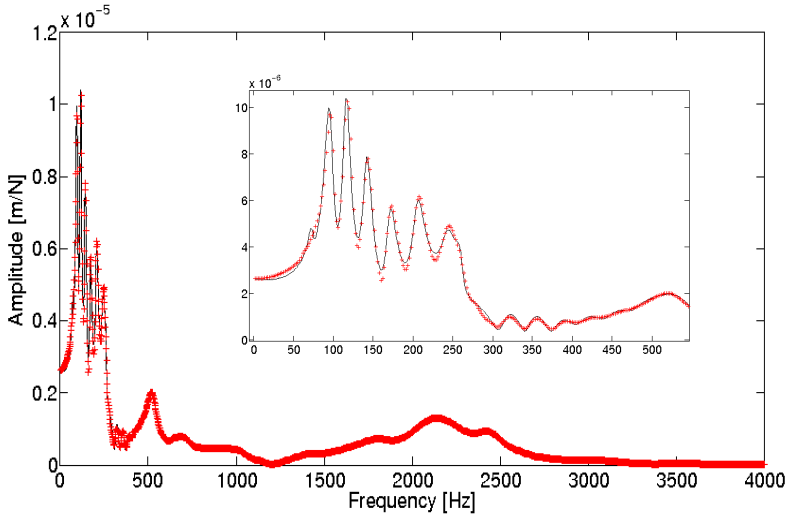

Figure A.10: Comparison between a Green's function ─ and its approximation -+- in the least favorable case.

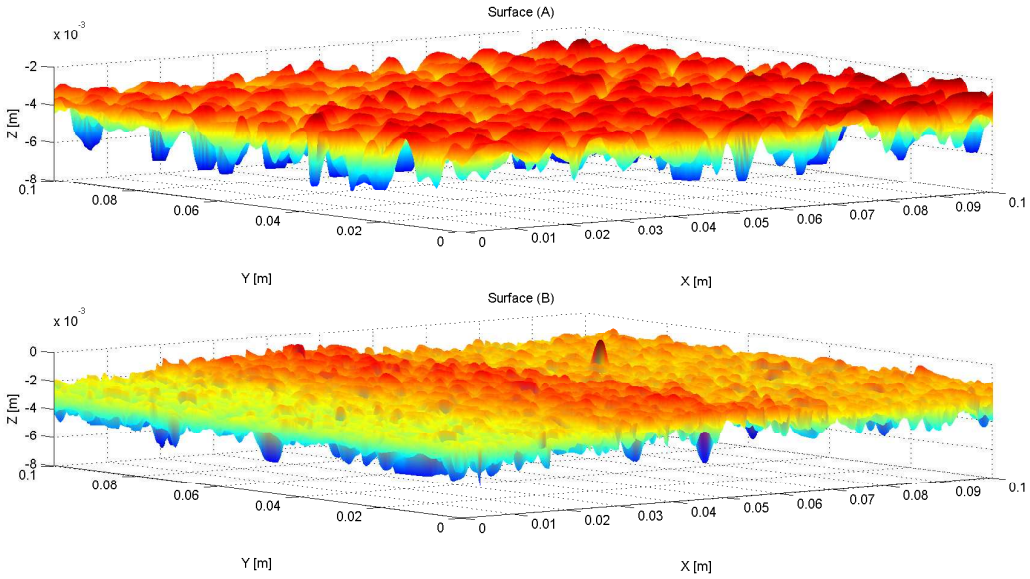

Figure A.11: 3*D* texture of two roads: (A) upper figure and (B) lower figure.

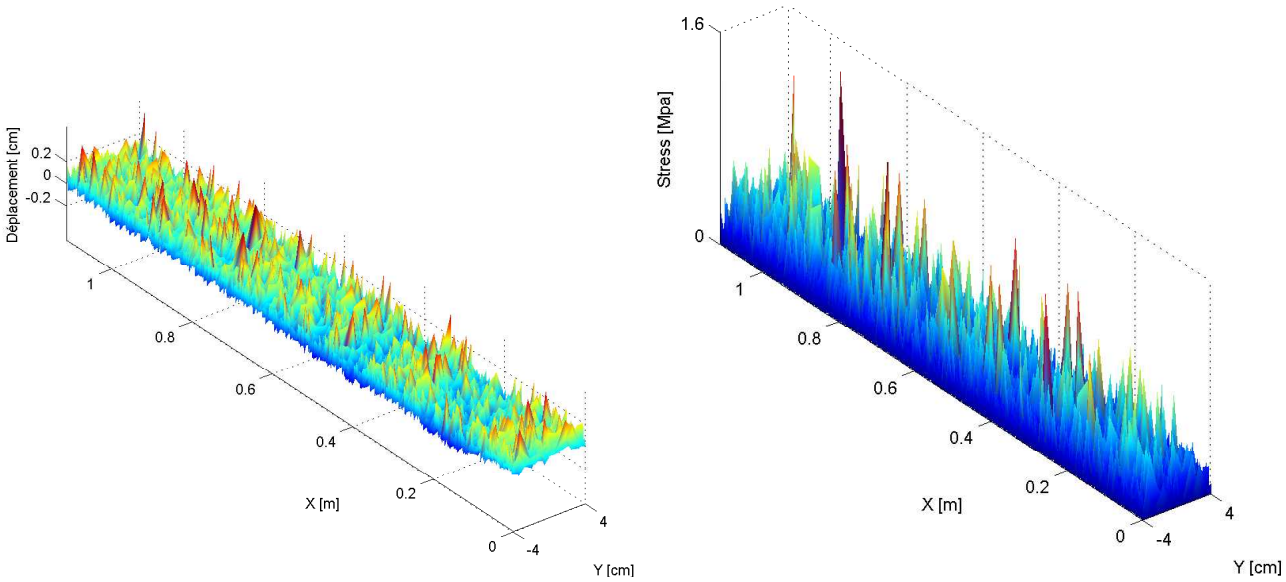

Figure A.12: Displacements and stress for road (A) and for points such that $x_0 = 0$ with $V_0 = 90\ km/h$.

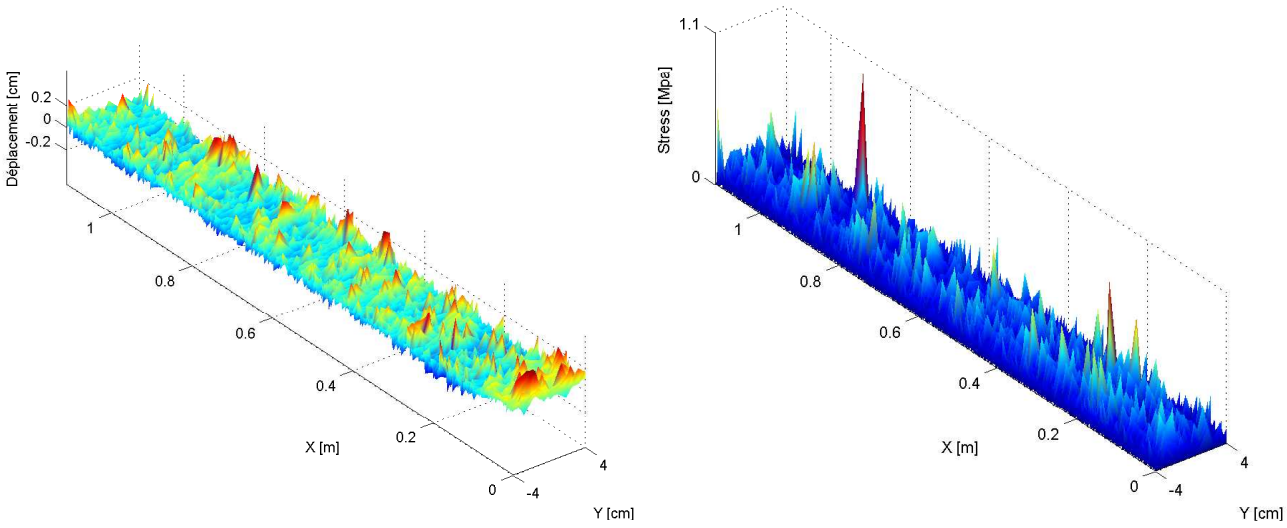

Figure A.13: Displacements and stress for road (B) and for points such that $x_0 = 0$ with $V_0 = 90\ km/h$.

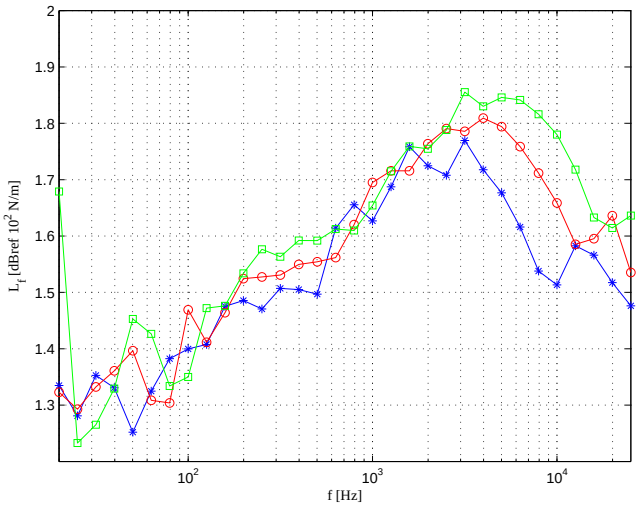

Figure A.14: 1/3 octave spectrum of the contact stress at point ($x_0 = 0, y_0 = 0$) for road (A) and for the velocities : -*- $V_0 = 50\ km/h$, -o- $V_0 = 70\ km/h$, -□- $V_0 = 90\ km/h$.

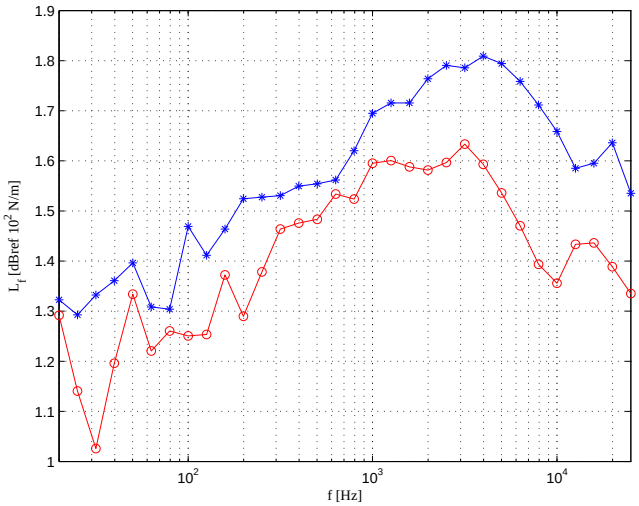

Figure A.15: 1/3 octave spectrum of the contact stress at 70 km/h, in point ($x_0 = 0, y_0 = 0$) : -*- road (A),-o- road (B).

M[Kg]	K[N/m]	ξ	k_c[N/m]
1	$4\ 10^5$	0.02	10^7

Table A.1: SDoF parameters used in the simulations

Time step [ms]	N_t	Standard convolution		Modal decomposition	
		N_g	Computing time [s]	N_m	Computing time [s]
0.1	2000	1900	0.06	1	0.02
0.1	20000	1900	1.01	1	0.10
0.01	20000	19000	5.50	1	0.15
0.01	200000	19000	105.14	1	1.50

Table A.2: Comparison of the computing times between standard convolutions and fast convolutions

Internal diameter	13” (330.2 *mm*)
Width of the tread	165 *mm*
Height of the sidewall	65 *mm*

Table A.3: Properties of tire Michelin 165/65/R13 77T.

Part	Material	Property	Value
Tread pattern	Rubber	ρ	1000 kg/m^3
		E	7 MPa
		ν	0.49
Bead	Steel	ρ	7850 kg/m^3
		E	162.6 GPa
		ν	0.33
Sidewall	Rubber +nylon belt	ρ	1000 kg/m^3
		E	109 MPa
		ν	0.48
Tread	Rubber +steel belt	ρ	2014 kg/m^3
		E_r	663 MPa
		E_x	624 MPa
		ν_{ry}	0.4
		G_{ry}	330 MPa

Table A.4: Mechanical properties of the tire.